Flexible Titanium Nitride/Germanium-Tin Photodetectors Based on Sub-Bandgap Absorption

Shu An,[1] *Yikai Liao,*[1] *and Munho Kim*[1,*]

[1]School of Electrical and Electronic Engineering, Nanyang Technological University, 50 Nanyang Avenue, 639798 Singapore, Singapore
*Email: munho.kim@ntu.edu.sg

Keywords: flexible photodetector, sub-bandgap, TiN, GeSn, strain

Abstract

We report an enhanced performance flexible titanium nitride/germanium-tin (TiN/GeSn) photodetector (PD) with extended photodetection range based on sub-bandgap absorption. Transfer-printed single-crystalline GeSn membranes are integrated with plasmonic TiN to form TiN/GeSn heterojunction on polyethylene terephthalate substrates. Formation of the heterojunction creates Schottky contact between TiN and GeSn. Schottky barrier height of 0.49 eV extends the photodetection wavelength to 2530 nm and further enhances the light absorption capability within the detection range. In addition, finite-difference time-domain simulation proves that the integration of TiN and GeSn could enhance average absorption from 0.13 to 0.33 in near infrared (NIR) region (e.g., 1400 to 2000 nm) and more than 70% of light is absorbed in TiN. Responsivity of the fabricated TiN/GeSn PDs is increased from 30 to 148.5 mA/W at 1550 nm. There is also a ~ 180 nm extension in optical absorption wavelength of the flexible TiN/GeSn PD. The enhanced performance of the device is attributed to the absorption and separation of plasmonic hot carriers via TiN and TiN/GeSn junction, respectively. The effect of external uniaxial strain is also investigated. Tensile strain of 0.3% could further increase the responsivity from 148.5 to 218 mA/W, while it is decreased to 102 mA/W by 0.25% compressive strain. In addition, the devices maintain stable performance after multiple and longtime bendings. Our results provide a robust and cost-effective method to extend the NIR photodetection capability of flexible group IV PDs.

1. Introduction

In recent years, germanium (Ge) has gained more popularity in near infrared (NIR) optoelectronics due to its high carrier mobility and absorption coefficient.[1–4] However, Ge photodetectors (PDs) are known to have significantly reduced responsivity when the wavelength becomes longer than 1.55 μm because the absorption coefficient of Ge abruptly drops beyond 1.55 μm. This limits its practical applications in L-band covering from 1560 to 1620 nm such as dense wavelength division multiplexing (DWDM).[5] Therefore, it is very important to develop a viable technology which can enhance the light absorption of Ge beyond 1.55 μm. Many attempts have been made to increase the responsivity of Ge PDs using a variety of strategies such as tensile strain introduced by stressor or mechanical bending,[6–8] artificially designed structure (e.g., resonant cavity, surface texturing, and integrated waveguide),[9–14] and optimization of pad design.[15] In addition, the integration of high Sn alloying to Ge is a promising candidate for high peak responsivity and detectivity in short wavelength infrared (SWIR) even to mid infrared (MIR) due to the efficient transition from indirect to direct bandgap.[16,17] Another practical method is sub-bandgap absorption that metallic layer absorbs the photons to generate hot carriers, followed by injection of hot carriers into GeSn through going over the SBH between GeSn and metal, which is usually smaller than the bandgap of GeSn. Dopant-mediated sub-bandgap Ge PDs with supersaturated concentration of gold (Au) have been reported, which are able to extend photo-response to SWIR region.[18] Therefore, it is worth exploring further how to couple sub-bandgap absorption into GeSn.

Noble metals such as Au and silver (Ag) are typical materials for hot carrier excitation owing to their high free carrier densities. However, the large work function of Au and Ag increases barrier height between metal and semiconductor, thus making it difficult to collect hot carriers. In addition, plasmon resonances of Au and Ag are narrow, which limit the broadband absorption. On the other hand, transparent conductive oxides,[19] carbides[20] and transition metal nitrides[21] offer the best choices for hot carriers excitation due to their metallic band structures and tunable plasmon resonances. In particular, titanium nitride (TiN), one of the transition metal nitrides, has attracted considerable attention as one of the most effective plasmonic metals by virtue of attractive optical properties and high photoelectric conversion efficiency. Specifically, it possesses small negative real part and high imaginary part of the permittivity that allow higher absorption than that of Au.[22] Its high melting point to sustain high optical power illumination enables high-performance hot-carrier devices.[23,24] It also exhibits high carrier concentration reaching to the order of 10^{22} cm^{-3}, which is necessary for

plasmon production in the visible and NIR ranges. Therefore, plasmonic Schottky PD with TiN has been a topic of interest in recent years. For example, TiN/Ge Schottky PD was demonstrated by Shindo *et al.* in 2019.[25] The authors deposited both Ge and TiN layers using a sputtering process to form the TiN/Ge heterojunction, then, achieved the photodetection up to 2600 nm. However, the deposited Ge was amorphous, causing poor device performance such as low responsivity. In addition, the device was built on rigid SiO_2/Si substrates, thus limiting its use in flexible and wearable applications.

In this paper, we have experimentally demonstrated the extension of the photodetection wavelength range of flexible sub-bandgap TiN/GeSn PDs. A 30 nm thick TiN film was sputtered on single-crystalline GeSn membranes transfer-printed on polyethylene terephthalate (PET) substrates to form flexible TiN/GeSn heterojunction. Schottky barrier height (SBH) of 0.49 eV was formed between TiN and GeSn, enabling the transition of photo-excited carriers resulted from the absorption in TiN. Therefore, a ~180 nm extension of the absorption wavelength coverage was observed, while at the same time displaying a significant enhancement in the responsivity over a wavelength range of 1400 to 2000 nm. In addition, external uniaxial strain further modulated the responsivity by changing the bandgap of GeSn and therefore its absorption coefficient. Overall, our results provide a viable approach to enhance the performances of flexible NIR PDs with broad spectral responsivity.

2. Results and Discussion

2.1 Device fabrication

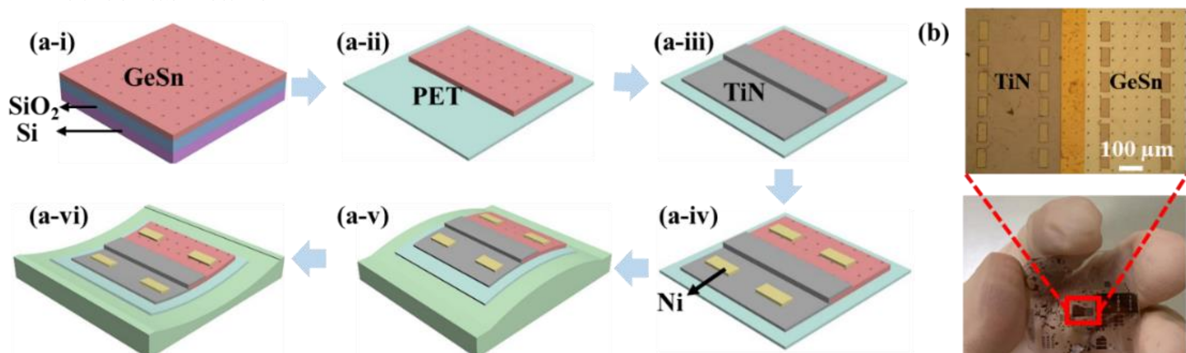

Fig. 1 (a) The schematic process flow of flexible TiN/GeSn heterojunction PDs: (a-i) Formation of etching hole array to facilitate subsequent undercut process. (a-ii) HF undercut to release GeSn membranes, followed by flip-transferring on PET substrate. (a-iii) Formation of rectangular-shaped heterojunction by sputtering TiN. (a-iv) Deposition of Ni contacts. (a-v)&(a-vi) Application of external uniaxial tensile and compressive strains by concave and convex bending fixtures, respectively. (b) An optical image of flexible TiN/GeSn PDs and its zoomed in microscopic image.

Fig. 1 outlines the fabrication procedure of flexible TiN/GeSn heterojunction PDs. Preparation of GeSn-on-insulator (GeSnOI) wafer began with the epitaxial growth of GeSn on Si and wafer bonding of GeSn/Ge/Si and oxidized Si substrates. 90 nm thick GeSn layer was epitaxially

grown on Ge-buffered Si substrates by metal organic chemical vapor deposition (MOCVD). Then, backside Si of GeSn/Ge/Si substrate was completely removed by potassium hydroxide (KOH) chemical etching and Ge was removed by reactive ion etching (RIE). GeSnOI consists of top 90 nm GeSn and bottom 300 nm SiO_2 on Si substrates. The detailed fabrication process and material characterization are described elsewhere.[26,27] Square-shaped membrane (2 × 2 mm^2) with etching hole array with a diameter and spacing of 3 and 50 µm, respectively, was patterned on GeSnOI, followed by chlorine (Cl_2) RIE to expose buried oxide layer (Fig. 1(a-i)). The etching holes facilitate the access of etching solution to sacrificial layer, leading to efficient undercut process. Subsequently, the sample was immersed in hydrofluoric acid (HF, 49%) for 2 minutes to completely remove the sacrificial SiO_2 layer. Released p-type GeSn membranes were flip-transferred on SU-8 2002 coated 175 µm thick PET substrates (Fig. 1(a-ii)). 30 nm thick TiN was sputtered on GeSn to form TiN/GeSn heterojunction (Fig. 1(a-iii)). Finally, nickel (Ni) pads (width: 40 µm and length: 80 µm) with a thickness of 30 nm were deposited on both TiN and GeSn (Fig. 1(a-iv)). Fig. 1(b) shows the microscopic image of flexible TiN/GeSn PDs. The devices were conformally placed on convex and concave fixtures with the same radii to apply comparable uniaxial tensile and compressive strain (Fig. 1(a-v, a-vi)), which were evaluated by Raman spectroscopy (UHT S300 & WITEC). Flexible Ge and GeSn PDs without TiN were also fabricated to study the effect of TiN on device performance.

2.2 Optical characterization

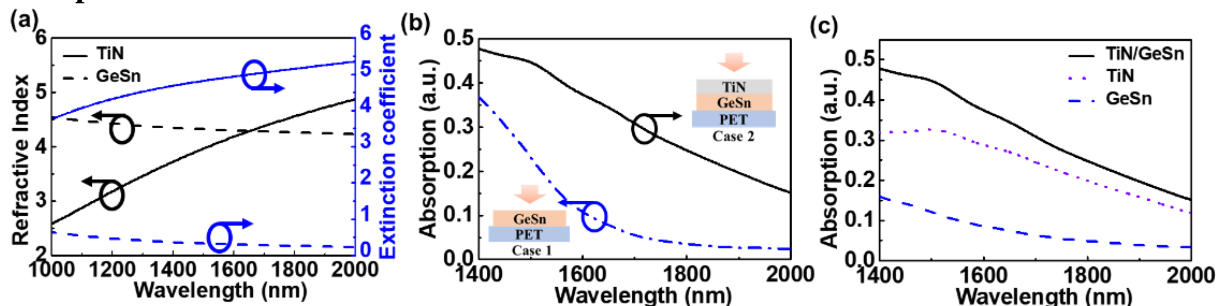

Fig. 2 (a) Refractive index and extinction coefficient of GeSn[28] (dash line) and thin TiN film (solid line). (b) Schematic of layer structures to simulate the light absorption and their corresponding simulated absorption: i) Case 1: GeSn membrane on PET ii): Case 2: TiN/GeSn membrane on PET. (c) Absorption in TiN (dot line) and GeSn (dash line) layers, respectively for Case 2.

Fig. 2(a) shows refractive index (n) and extinction coefficient (k) spectra of GeSn and TiN extracted from ellipsometry measurement, which matches well with previous reports.[2, 29,30] The refractive index of GeSn decreases slightly from 4.6 to 4.3 when the wavelength increases from 1000 to 2000 nm, while that of TiN gradually increases from 2.57 to 4.88. The refractive index spectra intersect at 1630 nm, indicating that GeSn possesses larger refractive index than TiN for wavelength below 1630 nm. Therefore, higher reflection occurs at GeSn surface due to high

refractive index contrast with air. In other words, low refractive index of TiN allows more photons to be absorbed due to reduced reflection.[31] The extinction coefficient of GeSn decreases from 0.6 to 0.2 when the wavelength increases from 1000 to 2000 nm, while TiN has much larger extinction coefficient varying from 4.5 to 5.5 at the same wavelength range. It indicates that TiN is an efficient absorber when it is integrated with GeSn.

To further investigate the effect of TiN layer on absorption, optical simulation was carried out using FDTD simulator (Lumerical). As shown in the inset of Fig. 2(b), the cross-sectional structure with the actual thicknesses (GeSn: 90 nm and TiN: 30 nm) and measured optical parameters (i.e. refractive index and extinction coefficient) of each layer were used. Fig. 2(b) shows the simulated absorption spectra of GeSn and TiN/GeSn, respectively. The absorption in TiN/GeSn heterojunction decreases steadily from 0.48 at 1400 nm to 0.12 at 2000 nm, while that of only GeSn decreases dramatically to 0.08 at 1650 nm followed by slightly decreases to 0.02. This indicates that addition of TiN broadens the absorption coverage spectrum. Meanwhile, it is clearly observed that the addition of TiN on top could enhance the average absorption from 0.13 to 0.33 in the range from 1400 to 2000 nm. Fig. 2(c) shows the simulated absorption of each structure. It is clearly shown that a considerable part of light is absorbed in TiN instead of GeSn due to its high extinction coefficient. To be more precise, the light absorbed in TiN is twice more than that in GeSn. Approximately 25% of total light power is absorbed in bottom GeSn, leading to the generation of free carrier in GeSn.

2.3 SBH measurement

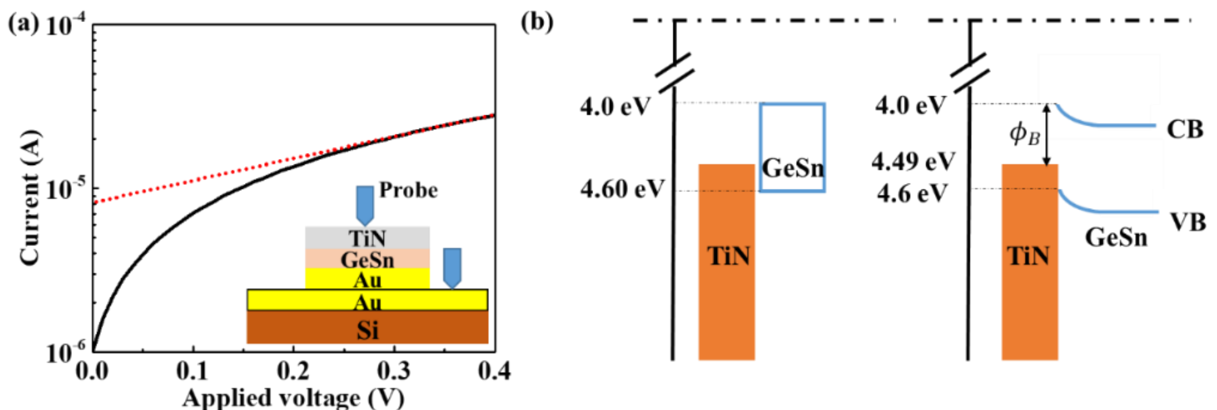

Fig. 3 (a) Current-voltage characteristic of TiN/GeSn Schottky diode. Red dash line represents the saturation current. Inset shows the cross-sectional structure of the device. (b) Band diagram of TiN/GeSn before and after junction formation.

To uncover enhancement mechanism in flexible TiN/GeSn PDs, SBH of TiN/GeSn heterojunction was measured at room temperature. A Schottky diode was built with top TiN/GeSn Schottky contact and bottom GeSn/Au ohmic contact. The contact between GeSn and Au is confirmed as Ohmic, as shown in Fig. S1. The device was placed on Ti/Au deposited

Si wafer for the backside contact. Fig. 3(a) shows the current-voltage characteristic of TiN/GeSn Schottky diodes under dark condition. The saturation current was extracted to be 8 μA. SBH can be calculated based on the following equation:

$$\Phi_B = \frac{k_B T}{q} \ln\left(\frac{A^* A T^2}{I_s}\right) \tag{1}$$

where k_B is the Boltzmann constant with value of 1.38×10^{-23} m^2 kg s^{-2} K^{-1}, T is the temperature in K, q is the electron charge, $A*$ is the Richardson's constant, A is the contact area in cm^2, and I_s is saturation current. The Richardson constant of Ge is 143 A/cm^{2}K^2 and the contact area is 100×100 μm^2.[32] Therefore, SBH between GeSn and TiN was extracted to be 0.49 eV, which agrees well with other reported values.[33,34] Fig. 3(b) shows the band diagram of TiN/GeSn heterojunction. The electron affinity and bandgap of GeSn with 8% Sn composition obtained from literatures are 4.0 and 0.60 eV, respectively.[32] The SBH of 0.49 eV indicates that the TiN/GeSn PD can detect the light at wavelengths as large as 2.53 μm. The photodetection wavelength range is comparable or larger compared with other reported GeSn based PDs with similar Sn composition.[35,36]

2.4 Photodetector characterization

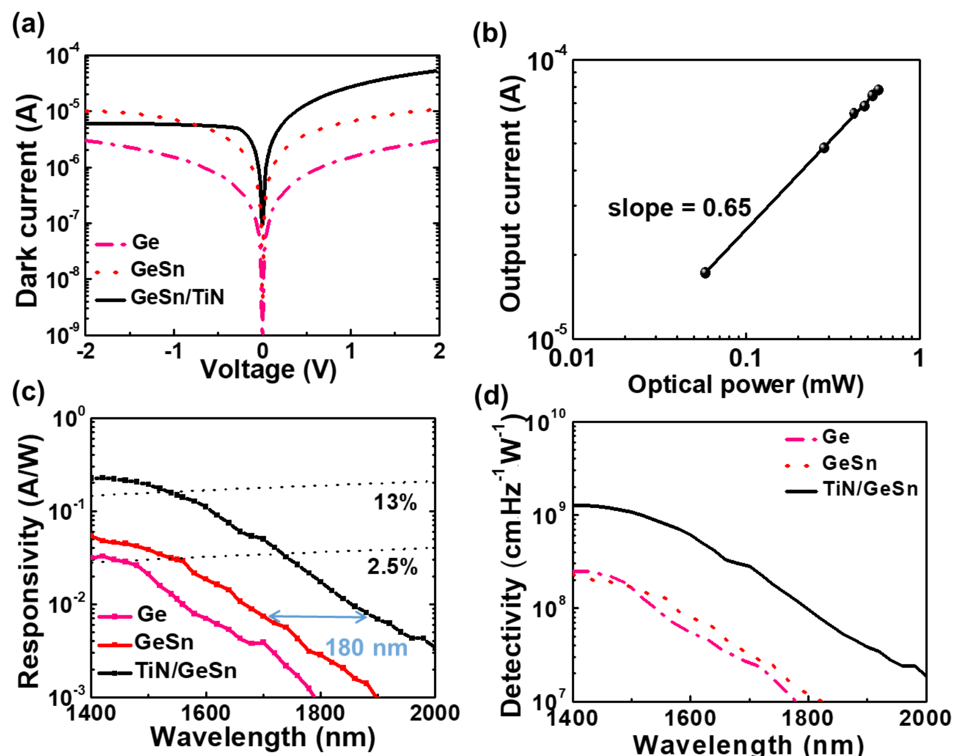

Fig. 4 (a) Dark current of flexible Ge, GeSn, and TiN/GeSn heterojunction PDs under flat condition. (b) Output current (i.e., photocurrent subtracted by dark current) as a function of the optical power at 1550 nm. The solid line represents a sublinear fitting of experimental data. (c) Spectral responsivity of flexible devices under flat condition at a bias of −2 V. Dotted line stands for various levels of external quantum efficiency. (d) Detectivity of flexible devices at a bias of −2 V.

The fabricated devices were characterized using a semiconductor parameter analyzer (Keithley 2450). Fig. 4 shows the optoelectronic characteristics of flexible TiN/GeSn PDs under flat condition. As shown in Fig. 4(a), dark current of flat Ge and GeSn PDs were symmetrical, while rectifying behavior was observed from flat TiN/GeSn PDs. Rectification ratio of larger than 10 at 2/-2 V was obtained, proving that stable Schottky junction was formed between TiN and GeSn. Ideality factor was calculated to be 1.66 as shown in Fig. S2, which is resulted from the electron-hole recombination in the depletion region, current mechanism owing to the large number of surface states.[9,37] This also explains the low rectification ratio shown in Fig. 4(a). In addition, the dark current density of TiN/GeSn PDs was calculated to be 28 mA/cm^2 at -2 V, which is comparable to those of other reported GeSn p-n junction PDs,[17,38] indicating high quality of the TiN/GeSn heterojunction.

Fig. 4(b) shows the output current as a function of various optical powers (i.e., 0.05, 0.28, 0.48, 0.54 and 0.58 mW) at 1550 nm. The output current increased from 17 to 78 μA with the increasing optical powers from 0.05 to 0.58 mW due to the enhanced electron-hole generation.[39,40] The relationship between output current and optical power can be expressed by the power law $I_{photo} \propto P^{\alpha}$. The slope of sublinear fitting line was extracted to be 0.65, indicating that deep level defect states reduced the photo response.[41]

We further characterized important figure-of-merits such as responsivity (R), external quantum efficiency (EQE), and detectivity (D*) to evaluate the optoelectronic performance. Responsivity is defined as the net photocurrent generated upon excitation of unit incident power. It can be calculated by the following equation

$$R = \frac{I_{photo} - I_{dark}}{P_{in}} \tag{2}$$

where I_{photo} is the photocurrent, I_{dark} is the dark current, P_{in} is the effective incident light power. EQE is defined as the number of effective photo-generated carriers upon excitation of per incident photon. It can be expressed with the following equation

$$EQE = \frac{Rhc}{\lambda q} \tag{3}$$

where h is the Planck constant, c is the speed of light in vacuum, λ is the photon's wavelength and q is the elementary charge. Detectivity is a commonly used parameter to assess the capability of the device to detect weak optical signal. For an ideal photodiode, noise in dark current is generally composed of thermal fluctuation and shot noise. Flicker or 1/f noise is excluded since its contribution is not significant for measurement conditions above 1 Hz. The

thermal noise is described as $I_{thermal} = \sqrt{4kT\Delta f / R_{shunt}}$ where k, T, and R_{shunt} are Boltzmann constant, absolute temperature, and shunt resistance, respectively.[42] The shunt noise calculated by the first derivative of bias voltage to dark current near 0 V was 40, 117, and 660 kΩ for GeSn/TiN, GeSn, Ge PDs, respectively.[43] The corresponding thermal noise is 6.3×10^{-13}, 3.7×10^{-13}, and 1.6×10^{-13} A·Hz$^{-1/2}$. The shot noise derived from $I_{shot} = \sqrt{2qI_{dark} / \Delta f}$ was 4×10^{-12}, 1.8×10^{-12}, and 1×10^{-12} A·Hz$^{-1/2}$, respectively.[42] The shot noise is one order magnitude higher than that of the thermal noise. Therefore, the shot noise is the dominant source to determine minimum detectable signal of the PDs at room temperature. Specific detectivity is calculated as[44]

$$D^* = \frac{\sqrt{A}R}{\sqrt{2qI_{dark}}} \tag{4}$$

where A is the effective light absorption area of the PD in units of cm^2. Fig. 4(c) presents the responsivity and EQE of the flat devices in the wavelength range from 1400 to 2000 nm at a bias of - 2 V. The incident power was 0.25 mW. The responsivity of the Ge PDs was continuously decreased with increasing wavelength due to a reduction of the absorption coefficient of Ge.[5] The responsivity of flexible GeSn PDs was enhanced from 11 to 30 mA/W at 1550 nm, which is attributed to band gap shrinkage from 0.66 to 0.6 eV of GeSn with 8% Sn content.[27] The responsivity of flat TiN/GeSn PDs was further enhanced to 148.5 mA/W, corresponding to an EQE of 13% at 1550 nm. The responsivity is comparable or higher than those of GeSn PDs.[25,45-47] Another significant enhancement is the ~180 nm extension of absorption coverage wavelength as indicated in arrows of Fig. 4(c), leading to the shift of cut-off wavelength towards to longer wavelength. As shown in Fig. 4(d), the detectivity of flat TiN/GeSn PDs at 1550 nm was calculated to be 8×10^{8} cm·Hz^{-1}·W^{-1}, which is eight times increase over that of flat GeSn PDs. Although the absorption layer of this flexible device is very thin, its detectivity is as good as those of other rigid GeSn PDs.[48,49] In addition, it should exhibit fast photo-switching response time due to high mobility of single crystalline GeSn.[8, 35, 50-53] These results suggest that the formation of stable TiN/GeSn Schottky junction is responsible for the observed enhancement in various figure-of-merits of TiN/GeSn PDs.

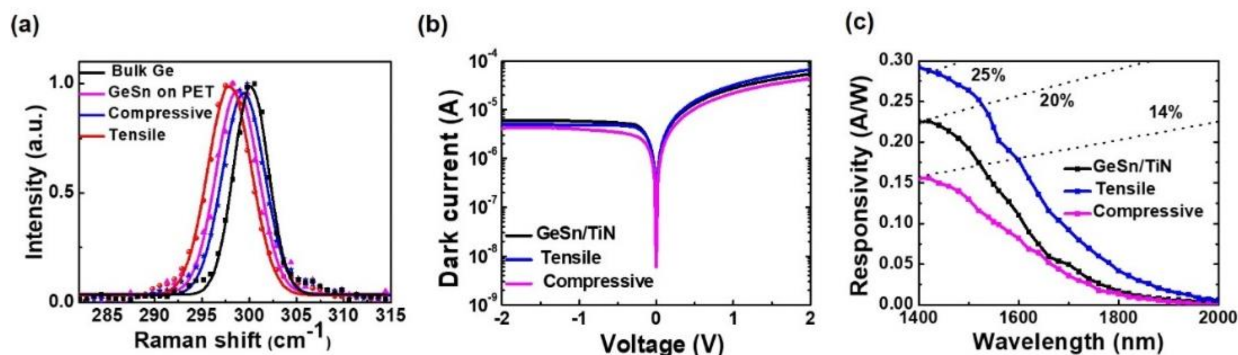

Fig. 5 (a) Raman spectra of GeSn membranes under flat and bent conditions. (b) Dark current of flexible TiN/GeSn PDs under flat and bent conditions. (c) Spectral responsivity of TiN/GeSn under flat and bent conditions. Dotted line stands for various levels of external quantum efficiency.

We further investigated the influence of mechanical uniaxial strains on the performance of flexible PDs. Strain values applied in GeSn membranes were characterized by Raman spectroscopy (UHT S300 & WITEC) with a 532 nm incident laser (corresponding to a penetration depth of 20 nm in Ge) focused on a 1 μm diameter spot. Fig. 5(a) shows the Raman spectra of bulk Ge, GeSn membranes on PET under flat and bent conditions, respectively. The peak values were obtained by Gaussian fitting in the range from 285 to 315 cm^{-1}. The peak of GeSn membranes was measured at 298.73 cm^{-1}, which was 1.47 cm^{-1} red-shifted compared to the reference bulk Ge due to the Sn alloy.[54] The peak was further red-shifted to 297.92 cm^{-1}, corresponding to a uniaxial tensile strain of 0.30% along <100> direction.[55] On the contrary, the Raman peak was blue shifted to 299.40 cm^{-1}, proving that 0.25% compressive was applied.

Fig. 5(b) shows the dark current of flexible TiN/GeSn PDs under flat and bent conditions at a bias range from – 2 to 2 V. It should be noted that the dark current was stable under bent conditions, indicating that strain resulted in negligible influence on the electrical performance of devices, which is quite different from that of GeSn metal-semiconductor-metal (MSM) PDs.[27] The major component of dark current is the carrier injection over SBH formed in the junction of TiN and GeSn. Tensile (compressive) strain could change the band structure of GeSn by moving down (up) its Γ-conduction band. Our calculation based on 30 k.p band model indicated that uniaxial tensile strain reduced the bandgap by 13 meV, while compressive strain increased the bandgap by 8 meV.[56] The influence of strain modulated bandgap of GeSn is negligible because the change value (i.e., (3% of the SBH)) is much smaller than SBH.

Fig. 5(c) shows the measured responsivity of bent TiN/GeSn PDs. The responsivity at 1550 nm increased from 149 to 218 mA/W with the tensile strain of 0.30%, while decreased to 102 mA/W with the compressive strain of 0.25%. The bandgap of GeSn was reduced from 597 to 584 meV with applied tensile strain, leading to enhanced absorption coefficient and higher responsivity. As discussed in Fig. 2(c), 25% of photocurrent was generated by photon excited

carriers in GeSn layer. Moreover, the change of absorption in TiN under strained condition is negligible due to its metallic property. Therefore, the modulation of the responsivity is attributed to the strain-induced changes in the absorption coefficient of GeSn. This should explain why the responsivity change modulated by strain is much smaller than that of GeSn MSM PD.[27]

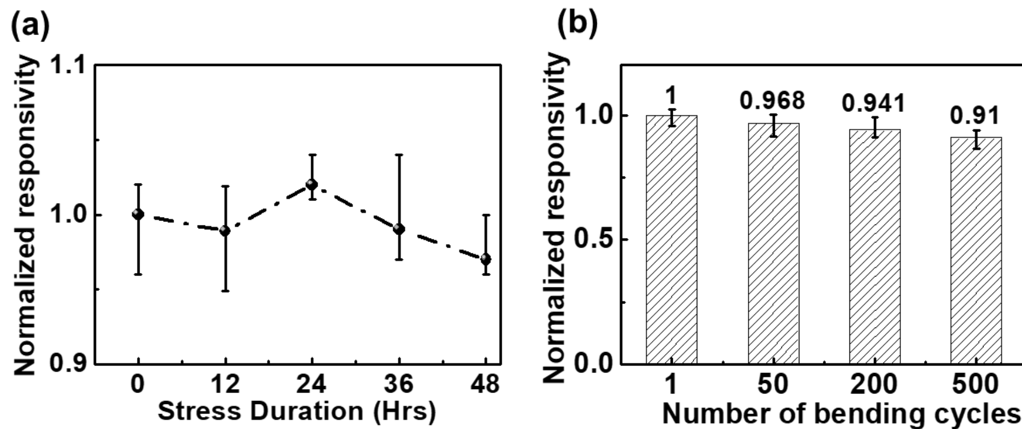

Fig. 6 (a) Normalized responsivity of the bent devices after 12, 24, 36, and 48 hours. (b) Responsivity of the PDs under 30 mm bending radius at 1550 nm after multiple bending cycles.

Fig. 6(a) shows responsivity measured under bent condition after 12, 24, 36, and 48 hours. Small variation of the responsivity proves that the device has no obvious degradation under a long time uniaxial strain. The excellent durability of optoelectronic performance of the PDs was demonstrated after multiple mechanical deformations as shown in Fig. 6(b). The device was bent on the convex fixture for 1, 50, 200, and 500 times, respectively. The responsivity remained the same with acceptable deviations after multiple bending.

3. Conclusion

In summary, we have demonstrated a flexible sub-bandgap TiN/GeSn PD based on the hetero-integration of single-crystalline GeSn membranes and plasmonic TiN. The FDTD simulation confirms that 30 nm TiN is able to enhance average absorption from 0.13 to 0.33 at the wavelength range of 1400 to 2000 nm. 0.49 eV of SBH is experimentally obtained at TiN/GeSn junction. Therefore, the responsivity at 1550 nm is greatly enhanced from 30 to 148.5 mA/W. In addition, the absorption coverage wavelength is red-shifted by 180 nm. Moreover, 0.3% uniaxial tensile strain further increases the responsivity to 218 mA/W, while 0.25% uniaxial compressive strain decreases the peak responsivity to 102 mA/W. Overall, the sub-bandgap absorption via TiN/GeSn provides a viable approach to achieve high-performance flexible group IV PDs with the extension of detection wavelength range.

4. Methods

Device fabrication: GeSnOI substrate with top 90 nm GeSn and middle 300 nm SiO_2 was thoroughly cleaned by Acetone, IPA, and DI water with sonication. Etching hole array (diameter: 3 µm and diameter: 50 µm) was patterned on GeSnOI by chlorine (Cl_2) RIE to etch down to buried oxide layer. Then, the sample was immersed in 49% HF for 2 minutes to completely remove the sacrificial SiO_2 layer and therefore release GeSn membranes, which were transferred on SU-8 2002 coated 175 µm thick PET substrates. TiN with a thickness of 30 nm was deposited on GeSn to form TiN/GeSn heterojunction by Evatec Cluster CLC200 Sputterer. Finally, 30 nm thick Ni pads (width: 40 µm and length: 80 µm) were deposited on both TiN and GeSn using e-beam evaporator (Edwards Auto306).

Optical characterization: The refractive index (n) and extinction coefficient (k) of TiN were measured by spectroscopic ellipsometer (J.A.Woolam Spectroscopic Ellipsometer). The absorption simulation was conducted by finite-difference time domain (FDTD) platform based on the real thickness of structures and extracted refractive and extinction coefficient of each layer.

Device Characterization: The fabricated devices were characterized using homemade setup, including a semiconductor parameter analyzer (Keithley 2450), a microscope, a probe platform, and a tunable laser (MF12L2-InF3) with a wavelength range and a beam size of 1.4 to 2 µm and 100 µm, respectively. The strains applied by bending were evaluated by Raman spectroscopy (UHT S300 & WITEC) with a 532 nm incident laser focused on a 1 µm diameter spot.

Conflicts of interest

There are no conflicts to declare.

Acknowledgement

This work was supported by the A∗STAR, Singapore, Advanced Manufacturing and Engineering (AME) Young Individual Research Grant (YIRG) under the Project A2084c0066 and Ministry of Education, Singapore, under the Grant ACRF Tier 2 grant (T2EP50120-0003). Authors acknowledge Xiao Gong at National University of Singapore and Bongkwon Son and Chuan Seng Tan at Nanyang Technological University for their technical support. Authors also acknowledge the support of Nanyang NanoFabrication Centre (N2FC).

References

1 Pillarisetty, R. Academic and Industry Research Progress in Germanium Nanodevices. *Nature* **2011**, 479 324.

2 Kim, M.; Liu, S.-C.; Kim, T. J.; Lee, J.; Seo, J.-H.; Zhou, W.; Ma, Z. Light Absorption Enhancement in Ge Nanomembrane and Its Optoelectronic Application. *Opt. Express* **2016**, 24, 16894.

3 Li, X.; Peng, L.; Liu, Z.; Liu, X.; Zheng, J.; Zuo, Y.; Xue, C.; Cheng, B. High-Power Back-to-Back Dual-Absorption Germanium Photodetector. *Opt. Lett.* **2020**, 45, 1358.

4 Michel, J.; Liu, J.; Kimerling, L. C. High-Performance Ge-on-Si Photodetectors. *Nat. Photonics* **2010**, 4, 527.

5 Palik, E. D. Handbook of Optical Constants of Solids. Vol. 3, *Academic press*, **1998,** pp.519-538.

6 Jain, J. R.; Hryciw, A.; Baer, T. M.; Miller, D. A.; Brongersma, M. L.; Howe, R. T. A Micromachining-Based Technology for Enhancing Germanium Light Emission Via Tensile Strain. *Nat. Photonics* **2012**, 6, 398.

7 Kim, M.; Seo, J.-H.; Yu, Z.; Zhou, W.; Ma, Z. Flexible Germanium Nanomembrane Metal-Semiconductor-Metal Photodiodes. *Appl. Phys. Lett.* **2016**, 109, 051105.

8 An, S.; Wu, S.; Lee, K.-H.; Tan, C. S.; Tai, Y.-C.; Chang, G.-E.; Kim, M. High-Sensitivity and Mechanically Compliant Flexible Ge Photodetectors with a Vertical P–I–N Configuration. *ACS Appl. Electron. Mater.* **2021**, 3, 1780.

9 Ghosh, S.; Lin, K.-C.; Tsai, C.-H.; Lee, K. H.; Chen, Q.; Son, B.; Mukhopadhyay, B.; Tan, C. S.; Chang, G.-E. Resonant-Cavity-Enhanced Responsivity in Germanium-on-Insulator Photodetectors. *Opt. Express* **2020**, 28, 23739.

10 Kim, M.; Yi, S.; Kim, J. D.; Yin, X.; Li, J.; Bong, J.; Liu, D.; Liu, S.-C.; Kvit, A.; Zhou, W.; Wang, X.; Yu, Z.; Ma, Z.; Li, X. Enhanced Performance of Ge Photodiodes via Monolithic Antireflection Texturing and α-Ge Self-Passivation by Inverse Metal-Assisted Chemical Etching. *ACS Nano* **2018**, 12, 6748.

11 Xia, Z.; Song, H.; Kim, M.; Zhou, M.; Chang, T.-H.; Liu, D.; Yin, X.; Xiong, K.; Mi, H.; Wang, X.; Xia, X.; Yu, Z.; Ma, Z.; Gan, Q. Single-Crystalline Germanium Nanomembrane Photodetectors on Foreign Nanocavities. *Sci. Adv.* **2017**, 3, e1602783.

12 Cho, M.; Seo, J.-H.; Kim, M.; Lee, J.; Liu, D.; Zhou, W.; Yu, Z.; Ma, Z. Resonant Cavity Germanium Photodetector Via Stacked Single-Crystalline Nanomembranes. *J. Vac. Sci. Technol. B* **2016**, 34, 040604.

13 Ren, F.-F.; Ang, K.-W.; Song, J.; Fang, Q.; Yu, M.; Lo, G.-Q.; Kwong, D.-L. Surface Plasmon Enhanced Responsivity in a Waveguided Germanium Metal-Semiconductor-Metal Photodetector. *Appl. Phys. Lett.* **2010**, 97, 091102.

14 Gosciniak, J.; Rasras, M. High-Bandwidth and High-Responsivity Waveguide-Integrated Plasmonic Germanium Photodetector. *JOSA B* **2019**, 36, 2481.

15 Zhao, X.; Moeen, M.; Toprak, M.; Wang, G.; Luo, J.; Ke, X.; Li, Z.; Liu, D.; Wang, W.; Zhao, C. Design Impact on the Performance of Ge PIN Photodetectors. *J. Mater. Sci. Mater. Electron.* **2020**, 31, 18.

16 Pham, T.; Du, W.; Conley, B.; Margetis, J.; Sun, G.; Soref, R.; Tolle, J.; Li, B.; Yu, S.-Q. Si - Based $Ge_{0.9}Sn_{0.1}$ Photodetector with Peak Responsivity of 2.85 A/W and Longwave Cutoff at 2.4 µm. *Electron. Lett.* **2015** 51, 854.

17 Tran, H.; Pham, T.; Margetis, J.; Zhou, Y.; Dou, W.; Grant, P. C.; Grant, J. M.; Al-Kabi, S.; Sun, G.; Soref, R. A. Si-Based GeSn Photodetectors toward Mid-Infrared Imaging Applications. *ACS Photonics* **2019**, 6, 2807.

18 Gandhi, H. H.; Pastor, D.; Pastor, T. T.; Kalchmair, S.; Smilie, L.; Mailoa, J. P.; Milazzo, R.; Napolitani, E.; Loncar, M.; Williams, J. S. Gold-Hyperdoped Germanium with Room-Temperature Sub-Band-Gap Optoelectronic Response. *Phys. Rev. Appl.* **2020**, 14, 064051.

19 Ishii, S.; Dao, T. D.; Chen, K.; Nagao, T. Transparent Oxides Forming Conductor/Insulator/Conductor Heterojunctions for Photodetection. *Nanotechnology* **2015**, 26, 215203.

20 Li, R.; Zhang, L.; Shi, L.; Wang, P. MXene Ti_3C_2: An Effective 2D Light-to-Heat Conversion Material. *ACS Nano* **2017**, 11, 3752.

21 Ishii, S.; Shinde, S. L.; Jevasuwan, W.; Fukata, N.; Nagao, T. Hot Electron Excitation from Titanium Nitride Using Visible Light. *ACS Photonics* **2016**, 3, 1552.

22 Chang, C.-C.; Nogan, J.; Yang, Z.-P.; Kort-Kamp, W. J.; Ross, W.; Luk, T. S.; Dalvit, D. A.; Azad, A. K.; Chen, H.-T. Highly Plasmonic Titanium Nitride by Room-Temperature Sputtering. *Sci. Rep.* **2019**, 9, 1.

23 Ishii, S.; Shinde, S. L.; Nagao, T. Nonmetallic Materials for Plasmonic Hot Carrier Excitation. *Adv. Opt. Mater.* **2019**, 7, 1800603.

24 Dal Forno, S.; Lischner, Electron-Phonon Coupling and Hot Electron Thermalization in Titanium Nitride. *Phys. Rev. Mater*. **2019**, 3, 115203.

25 Shinde, S. L.; Ishii, S.; T. Nagao, Sub-Band Gap Photodetection from the Titanium Nitride/Germanium Heterostructure. *ACS Appl. Mater. Interfaces* **2019**, 11, 21965.

26 Lei, D.; Lee, K. H.; Bao, S.; Wang, W.; Wang, B.; Gong, X.; Tan, C. S.; Yeo, Y.-C. GeSn-on-Insulator Substrate Formed by Direct Wafer Bonding. *Appl. Phys. Lett.* **2016**, 109, 022106.

27 An, S.; Wu, S.; Tan, C. S.; Chang, G.-E.; Gong, X.; Kim, M. Modulation of Light Absorption in Flexible GeSn Metal–Semiconductor–Metal Photodetectors by Mechanical Bending. *J. Mater. Chem. C* **2020**, 8, 13557.

28 Lieten, R. R.; Fleischmann, C.; Peters, S.; Santos, N. M.; Amorim, L. M.; Shimura, Y.; Uchida, N.; Maeda, T.; Nikitenko, S.; Conard, T. Structural and Optical Properties of Amorphous and Crystalline GeSn Layers on Si. *ECS J Solid State Sci Technol* **2014**, 3, P403.

29 Chu, H.; Gu, C.; Li, S.; Zhang, Y.; Bian, J.; Jiang, C. Measuring the Absorption of TiN Metallic Films Using Cathodoluminescence of GaN Films. *Opt. Mater. Express* **2017**, 7, 1302.

30 Pflüger, J.; Fink, J. In Handbook of Optical Constants of Solids. *Elsevier* **1997**, 293.

31 Mistrik, J.; Kasap, S.; Ruda, H. E.; Koughia, C.; Singh, J. Handbook of Electronic and Photonic Materials. *Springer* **2017**, 1.

32 Sze, S. M.; Li, Y.; Ng, K. K. Physics of Semiconductor Devices. *John wiley & sons* **2021,** pp.270-286.

33 Wu, H.; Huang, W.; Lu, W.; Tang, R.; Li, C.; Lai, H.; Chen, S.; Xue, C. Ohmic Contact to N-Type Ge with Compositional Ti Nitride. *Appl. Surf. Sci.* **2013**, 284, 877.

34 Yamamoto, K.; Mitsuhara, M.; Hiidome, K.; Noguchi, R.; Nishida, M.; Wang, D.; Nakashima, H. Role of an Interlayer at a TiN/Ge Contact to Alleviate the Intrinsic Fermi-Level Pinning Position toward the Conduction Band Edge. *Appl. Phys. Lett.* **2014**, 104, 132109.

35 Yang, F.; Yu, K.; Cong, H.; Xue, C.; Cheng, B.; Wang, N.; Zhou, L.; Liu, Z..Wang, Q. Highly Enhanced SWIR Image Sensors Based on $Ge_{1-x}Sn_x$–Graphene Heterostructure Photodetector. *ACS Photonics* **2019** 6, 1199-1206.

36 Conley, B. R.; Margetis, J.; Du, W.; Tran, H.; Mosleh, A.; Ghetmiri, S. A.; Tolle, J.; Sun, G.; Soref, R.; Li, B. Si Based GeSn Photoconductors with a 1.63 A/W Peak Responsivity and a 2.4 µm Long-Wavelength Cutoff. *Appl. Phys. Lett.* **2014** 105, 221117.

37 Janardhanam, V.; Jyothi, I.; Kim, Y.; Lee, S.-N.; Yun, H.-J.; Hong, W.-K.;Choi, C.-J. Carrier Conduction Mechanisms of WSe_2/P-Type Ge Epilayer Heterojunction Depending on the Measurement Temperature and Applied Bias. *J. Alloys Compd.* **2020** 842, 155843.

38 Zheng, J.; Wang, S.; Liu, Z.; Cong, H.; Xue, C.; Li, C.; Zuo, Y.; Cheng, Wang, B. Q. GeSn PIN Photodetectors with Gesn Layer Grown by Magnetron Sputtering Epitaxy. *Appl. Phys. Lett.* **2016**, 108, 033503.

39 Pataniya, P. M.; Patel, V.; Sumesh, C. MoS_2/WSe_2 Nanohybrids for Flexible Paper-Based Photodetectors. *Nanotechnology* **2021** 32, 315709.

40 Yu, M.-W.; Ishii, S.; Shinde, S. L.; Tanjaya, N. K.; Chen, K.-P.; Nagao, T. Direct Observation of Photoinduced Charge Separation at Transition-Metal Nitride–Semiconductor Interfaces. *ACS Appl. Mater. Interfaces* **2020** 12, 56562-56567.

41 Pataniya, P. M.; Late, D.; Sumesh, C. Photosensitive WS_2/ZnO Nano-Heterostructure-Based Electrocatalysts for Hydrogen Evolution Reaction. *ACS Appl. Energy Mater.* **2021** 4, 755-762.

42 Konczakowska, A.; Wilamowski, B. M. Noise in Semiconductor Devices. In Fundamentals of Industrial Electronics, *CRC Press*, **2018**, pp. 1-12.

43 Zhou, H.; Xu, S.; Lin, Y.; Huang, Y.-C.; Son, B.; Chen, Q.; Guo, X.; Lee, K. H.; Goh, S. C.-K.; Gong, X. High-Efficiency GeSn/Ge Multiple-Quantum-Well Photodetectors with Photon-Trapping Microstructures Operating at 2 μm. *Opt. Express* **2020** 28, 10280-10293.

44 Li, X.; Chen, X.; Li, S.; Chu, F.; Deng, W.; Zhang, X.; Li, J.; Bao, X.; An, B.; You, C. High Performance Sub-Bandgap Photodetection Via Internal Photoemission Based on Ideal Metal/2D-Material Van Der Waals Schottky Interface. *Nanoscale* **2021**.

45 Wang, L.; Zhang, Y.; Wu, Y.; Liu, T.; Miao, Y.; Meng, L.; Jiang, Z.; Hu, H. Effects of Annealing on the Behavior of Sn in Gesn Alloy and GeSn-Based Photodetectors. *IEEE Trans Electron Devices* **2020** 67, 3229-3234.

46 Ghosh, S.; Lin, K.-C.; Tsai, C.-H.; Kumar, H.; Chen, Q.; Zhang, L.; Son, B.; Tan, C. S.; Kim, M.; Mukhopadhyay, B. Metal-Semiconductor-Metal GeSn Photodetectors on Silicon for Short-Wave Infrared Applications. *Micromachines* **2020** 11, 795.

47 Atalla, M. R.; Assali, S.; Attiaoui, A.; Lemieux - Leduc, C.; Kumar, A.; Abdi, S.; Moutanabbir, O. All - Group IV Transferable Membrane Mid - Infrared Photodetectors. *Adv. Funct. Mater.* **2020**, 2006329.

48 Tran, H.; Du, W.; Ghetmiri, S. A.; Mosleh, A.; Sun, G.; Soref, R. A.; Margetis, J.; Tolle, J.; Li, B.; Naseem, H. A. Systematic Study of $Ge_{1-x}Sn_x$ Absorption Coefficient and Refractive Index for the Device Applications of Si-Based Optoelectronics. *J. Appl. Phys.* **2016**, 119, 103106.

49 Wu, S.; Xu, S.; Zhou, H.; Jin, Y.; Chen, Q.; Huang, Y.-C.; Zhang, L.; Gong, X.; Tan, C. S. High-Performance Back-Illuminated $Ge_{0.92}Sn_{0.08}$/Ge Multiple-Quantum-Well Photodetector on Si Platform for SWIR Detection. *IEEE J Sel Top Quantum Electron* **2021**.

50 Pataniya, P.; Zankat, C. K.; Tannarana, M.; Sumesh, C.; Narayan, S.; Solanki, G.; Patel, K.; Pathak, V.; Jha, P. K. Based Flexible Photodetector Functionalized by WSe_2 Nanodots. ACS *Appl. Nano Mater.* **2019** 2, 2758-2766.

51 Jeon, C.-W.; Lee, S.-S.; Park, I.-K. Flexible Visible-Blind Ultraviolet Photodetectors Based on ZnAl-Layered Double Hydroxide Nanosheet Scroll. *ACS Appl. Mater. Interfaces* **2019** 11, 35138-35145.

52 Takeuchi, W.; Taoka, N.; Kurosawa, M.; Sakashita, M.; Nakatsuka, O.; Zaima, S. High Hole Mobility Tin-Doped Polycrystalline Germanium Layers Formed on Insulating Substrates by Low-Temperature Solid-Phase Crystallization. *Appl. Phys. Lett.* **2015** 107, 022103.

53 Sadoh, T.; Kai, Y.; Matsumura, R.; Moto, K.; Miyao, M. High Carrier Mobility of Sn-Doped Polycrystalline-Ge Films on Insulators by Thickness-Dependent Low-Temperature Solid-Phase Crystallization. *Appl. Phys. Lett.* **2016** 109, 232106.

54 Gassenq, A.; Milord, L.; Aubin, J.; Pauc, N.; Guilloy, K.; Rothman, J.; Rouchon, D.; Chelnokov, A.; Hartmann, J.; Reboud, V. Raman Spectral Shift Versus Strain and Composition in GeSn Layers with 6%−15% Sn Content. *Appl. Phys. Lett.* **2017**, 110, 112101.

55 An, S.; Tai, Y.-C.; Lee, K.-C.; Shin, S.; Cheng, H.-H.; Chang, G.-E.; Kim, M. Raman Scattering Study of GeSn under < 1 0 0> and < 1 1 0> Uniaxial Stress. *Nanotechnology* **2021**, 32, 355704.

56 Song, Z.; Fan, W.; Tan, C. S.; Wang, Q.; Nam, D.; Zhang, D. H.; Sun, G. Band Structure of Strained $Ge_{1-x}Sn_x$ Alloy: A Full-Zone 30-Band *k-p* Model. *IEEE J Quantum Electron* **2019**, 56, 1.